Using quantitative magnetic resonance imaging to track cerebral alterations in multiple sclerosis brain: a longitudinal study

Nora Vandeleene[a], Camille Guillemin[a,b], Solène Dauby[a,c], Florence Requier[a,b], Maëlle Charonitis[a,b], Daphne Chylinski[a,b], Evelyne Balteau[a], Pierre Maquet[a,c], Emilie Lommers[a,c*], Christophe Phillips[a,d*]

[a] GIGA CRC in vivo Imaging, University of Liège, Liège, Belgium
[b] Psychology and Cognitive Neuroscience Research Unit, University of Liège, Liège, Belgium
[c] Clinical Neuroimmunology Unit, Neurology Department, CHU Liège, Belgium
[d] GIGA in silico Medicine, University of Liège, Liège, Belgium

* These authors equally contributed to the work.

Corresponding author: Christophe PHILLIPS
GIGA – CRC in vivo imaging B30
Allée du 6 août
4000 Liège
Belgium

Acknowledgements
The authors are particularly thankful for the patients who took part in this study.
N.V., E.L. and C.P. are supported by the Fonds de la Recherche Scientifique (F.R.S-FNRS Belgium).

Data availability
The data that support the findings of this study are available on request from the corresponding author. The data are not publicly available due to privacy or ethical restrictions.

Conflict interests
None.

Abbreviations:
ARoC: Annual Rate of Change, **BPF**: Brain Parenchymal Fraction, **CDP**: Confirmed Disability Progression, **cMRI**: Conventional Magnetic Resonance Imaging, **CNS:** Central

Nervous System, **GMF**: Grey Matter Fraction, **GLMM**: General Linear Mixed Model, **LF**: Lesion Fraction, **MPM**: Multi-Parameter Mapping, **MRI**: Magnetic Resonance Imaging, **MS**: Multiple Sclerosis, **MT**: Magnetization Transfer, **MTR**: Magnetization Transfer Ratio, **MTsat**: Saturated Magnetization Transfer, **NABT**: Normal Appearing Brain Tissue, **NACGM**: Normal Appearing Cortical Grey Matter, **NADGM**: Normal Appearing Deep Grey matter, **NAWM**: Normal Appearing White Matter, **NEDA-3**: No Evidence of Disease Activity, **RRMS**: Relapsing-Remitting Multiple Sclerosis, **PD**: Proton Density, **PMS**: Progressive Multiple Sclerosis, **qMRI**: Quantitative Magnetic Resonance Imaging, **R1**: Longitudinal Relaxation Rate (1/T1), **R2***: Transverse Relaxation Rate (1/T2*), **TIV**: Total Intracranial Volume, **TPM**: Tissue Probability Map, **US:** Unified Segmentation, **USwL**: Unified Segmentation with Lesion

Abstract

Quantitative MRI quantifies tissue microstructural properties and supports the characterization of cerebral tissue damages. With an MPM protocol, 4 parameter maps are constructed: MTsat, PD, R1 and R2*, reflecting tissue physical properties associated with iron and myelin contents. Thus, qMRI is a good candidate for *in* vivo monitoring of cerebral damage and repair mechanisms related to MS. Here, we used qMRI to investigate the longitudinal microstructural changes in MS brain.

Seventeen MS patients (age 25-65, 11 RRMS) were scanned on a 3T MRI, in two sessions separated with a median of 30 months, and the parameters evolution was evaluated within several tissue classes: NAWM, NACGM and NADGM, as well as focal WM lesions. An individual annual rate of change for each qMRI parameter was computed, and its correlation to clinical status was evaluated. For WM plaques, three areas were defined, and a GLMM tested the effect of area, time points, and their interaction on each median qMRI parameter value.

Patients with a better clinical evolution, i.e., clinically stable or improving state, showed positive annual rate of change in MTsat and R2* within NAWM and NACGM, suggesting repair mechanisms in terms of increased myelin content and/or axonal density as well as edema/inflammation resorption. When examining WM lesions, qMRI parameters within surrounding NAWM showed microstructural modifications, even before any focal lesion is visible on conventional FLAIR MRI.

The results illustrate the benefit of multiple qMRI data in monitoring subtle changes within normal appearing brain tissues and plaque dynamics in relation with tissue repair or disease progression.

Keywords:

Quantitative MRI, relaxometry, longitudinal analysis, multiple sclerosis.

Key points:

- Patients with a better clinical evolution showed microstructural improvement in term of MTsat and R2* increase in their normal appearing tissue, suggesting repair mechanisms.
- Using qMRI allows to detect modifications in tissue microstructure in normal appearing tissues surrounding lesions several months before they are visible on conventional MRI.

1. Introduction

Multiple sclerosis (MS) is a chronic autoimmune disease of the central nervous system (CNS). Plaques are the pathological hallmark of MS. They are spread in acute, focal, disseminated and recurrent way throughout the CNS and harbor variable degrees of inflammation, demyelination, gliosis and axonal injury [1, 2]. Plaques are not restricted to the white matter (WM), but are also present in the cortex and deep grey matter (GM) [3-5].

Over and above focal WM lesions, an early, diffuse and chronic inflammation within the normal appearing white matter (NAWM) and grey matter (NAGM) is ultimately responsible for diffuse neuro-axonal loss and neurodegeneration, which is deemed responsible for a progressive accumulation of disability [3, 4, 6].

By contrast, effective repair mechanisms can occur within focal lesions but probably also in normal appearing brain tissue (NABT) [7]. However, our understanding of these complex processes is still fragmentary. The difficulty of acquiring histopathological data on MS patients at various stages of the disease makes it challenging to describe the time course of injury and potential repair mechanisms in MS. Consequently, there is a need for new imaging techniques to improve the *in-vivo* monitoring of brain damages formation, progression and repair in MS [8].

Conventional MRI (cMRI) readily depicts focal WM lesions on T2/FLAIR sequences and is able to distinguish between acute and allegedly chronic lesions. T2-hyperintensities in cMRI constitute the keystone of McDonald diagnostic criteria [9] and also make an important contribution to the monitoring of WM lesion burden. Unfortunately, cMRI sequences do not sensitively detect cortical lesions and diffuse changes in NABT, due to a rather low sensitivity of cMR imaging for cortical lesions, mixed contrast weight, and an overall limited histopathological specificity within cerebral tissues. Quantitative MRI (qMRI) potentially

overcomes these limitations by quantifying physical microstructural properties of cerebral tissue in standardized units. qMRI is more sensitive but also more specific to microstructural properties of CNS tissues. Magnetization transfer ratio (MTR) was regularly linked to cerebral macromolecular content detected by a greater percentage loss of magnetization in voxels with a higher myelin content and axons density [10-12]. Post-mortem studies comparing the relative contribution of these two factors indicate that myelin has a stronger and more direct influence on MTR than the axonal density, which is considered as a T1-dependent effect. Tissue water content (inflammation, edema…), another T1-dependent effect, also accounts for MTR variability [11, 13, 14]. However, the MT saturation (MTsat) map offers a measure which, unlike MTR, is minimally affected by longitudinal relaxation and B1 mapping inhomogeneities [15], increasing its sensitivity to myelin content. Moreover, the brain contrast to noise ratio is larger for the MTsat map than for MTR, thus improving brain tissue segmentation in healthy subjects [11, 16]. R2* was usually linked to iron and myelin contents, as paramagnetic iron and diamagnetic myelin generate microscopic field gradients in the CNS, thus shortening T2* and increasing R2* (1/T2*). Orientation and density of myelin fibers are also a determining factor of R2* values [17-19]. Iron is probably a key factor in MS monitoring as it was shown that aberrant iron metabolism occurs in the course of the disease [20]. Particularly increased iron concentration within chronic active lesions (i.e iron rim lesion) or deep grey matter structures was observed [20]. Regarding the longitudinal relaxation rate R1 (1/T1), its three major determinants in the CNS are tissue myelination and associated axons, iron, and extracellular water contents [19, 21, 22]. Finally, proton density (PD) mostly reflects the free water content of the brain [23].

A number of cross-sectional studies using a combination of MT, R1, R2* or PD parameters, comparing MS patients to healthy controls, reported significant changes in the microstructure

of NABT, such as a decrease in MT, R1 and R2* and an increase in PD in patients [24-32]. Few studies addresses the longitudinal variations in qMRI. R2* [33-35], PD and T1 were reported to increase in the basal ganglia over a period of a year [36], whereas a decrease in MTR in NAWM was reported over one [37] or two years [38].

Regarding focal WM plaques, qMRI emerges as an appealing biomarker to describe the dynamic processes of demyelination and remyelination. For instance, MTR was shown to sharply decrease within gadolinium enhancing lesions before recovering during the subsequent months [39-41], and within NAWM days to weeks before the formation of a new active lesion [42, 43].

Because each qMRI parameter is differently sensitive to histologically measured iron and myelin contents, this approach might become a fundamental tool for longitudinal *in vivo* monitoring of MS lesions and NABT evolution at the tissue microstructural level.

In this longitudinal study, we investigate the evolution of four simultaneously acquired qMRI parameters (MTsat, PD, R1, R2*) within NABT and WM lesions of 17 MS patients - relapsing remitting (RRMS) and progressive MS (PMS) - who were scanned two times with at least a one-year interval, following the same multi-parameter mapping (MPM) protocol at 3 Tesla [10, 44].

We assessed the time course of parameter values in several tissue classes: normal appearing white matter (NAWM), normal appearing cortical and deep GM (NACGM and NADGM) as well as focal WM lesions. In addition, we related longitudinal qMRI changes within NABT to clinical course.

2. Materials and methods

2.1 Population

Seventeen patients, recruited at the specialized MS outpatient clinic of the CHU Liège, Belgium, with a diagnosis of MS according to the McDonald criteria 2010 [45], were gathered from two studies: ten of them were part of the work reported by Lommers et al. 2019 [24], the other seven were recruited from another MS study taking place at the GIGA Cyclotron Research Centre – In Vivo Imaging (Liège, Belgium) [46]. For the first study (10 subjects), the inclusion criteria were (1) age between 18 and 65 years ; (2) Expanded Disability Status Scale (EDSS) inferior or equal to 6.5 ; (3) absence of relapse within the previous four weeks ; (4) absence of IVMP administration for at least 6 months prior to the study. Both RRMS and PMS patients were recruited. The second study (7 subjects) differs a bit as it comprises only RRMS patients, and the inclusion criteria were (1) age between 18 and 45, (2) EDSS between 0 and 4, (3) absence of relapse for at least 6 months prior to the study, (4) disease duration was below or equal to 5 years, (5) absence of IVMP administration for at least 6 months prior to the study. For both studies, compatibility with MRI and absence of other neurological/psychiatric diseases were required. These studies were approved by the local ethics committee (approval numbers B707201213806 and B707201835630, respectively). All patients were followed up and scanned twice on the same 3T MRI scanner, every 1 to 3 years. For each of the 17 MS patients, data from two MRI sessions were available, at T0 and T1. This cohort included 11 RRMS and 6 (primary and secondary) PMS patients. Thirteen were receiving disease-modifying treatments (DMTs). The patients' median age was 36 years (range: 25-65) and the median time interval between two scans was 30 months (range: 14-61). Demographic data appears in Table 1. Extended individual information appears in Supplementary data.

2.2 MR image acquisition

MRI data were acquired on a 3T whole-body MRI-scanner (Magnetom Prisma, Siemens Medical Solutions, Erlangen, Germany). The whole-brain MRI acquisitions included a multi-parameter mapping protocol (MPM), from which one can simultaneously estimate (semi)quantitative maps of magnetization transfer saturation (MTsat), proton density (PD), transverse relaxation (R1) and effective longitudinal relaxation (R2*). This protocol arising from an international collaborative effort [10, 44], has already been used to study brain microstructure in various conditions including normal aging [9, 44, 47], brain tumor [48], Parkinson's disease [49-51] as well as MS. It consists of three co-localized 3D multi-echo fast low angle shot (FLASH) acquisitions at $1mm^3$ resolution and two additional calibration sequences to correct for inhomogeneities in the RF transmit field [52, 53]. The FLASH datasets were acquired with predominantly PD, T1 and MT weighting, referred to in the following as PDw, T1w and MTw, at multiple echo times. All three had high bandwidth to minimize off-resonance and chemical shift artifacts. Volumes were acquired in 176 sagittal slices using a 256x224 voxel matrix. GRAPPA parallel imaging was combined with partial Fourier acquisition to speed up acquisition time to approximately 20 min. An additional FLAIR sequence was recorded with spatial resolution $1mm^3$ and TR/TE/TI=5000ms/516ms/1800ms. Extra B1 field mapping images (transmit B1+ and receive B1- fields) were also acquired to reduce spatial inhomogeneities related to B1 effect. This was essential for proper quantification of T1 (or R1=1/T1) in particular. Finally, B0 field mapping images, corresponding to both magnitude images and pre-subtracted phase image, were acquired for image distortions corrections. A summary of the acquisition parameters appears in Supplementary data.

Note that these MR sequences at 3 Tesla are not sensitive to cortical lesion as described in [54, 55] although a few lesions at the cortico-subcortical border were detected. Quantification of cortical parameters is thus confounded by voxels potentially located within cortical lesions.

2.3 MR image processing

All data processing was performed in Matlab (The MathWorks Inc., Natick, MA, USA) using SPM12 (www.fil.ion.ucl.ac.uk/spm) and three additional dedicated SPM extensions: the Lesion Segmentation Tool (LST) version 1.2.3 (www.statisticalmodelling.de/lst.html) [56], the "quantitative MRI and in vivo histology using MRI" toolbox (hMRI, http://hmri.info) [10], and "US-with-Lesion" tool (USwL, https://github.com/CyclotronResearchCentre/USwLesion).

Quantitative maps - MTsat, PD, R1 and R2* - were estimated using the hMRI toolbox. T1w, PDw and MTw images acquired at multiple echo times (TE) were extrapolated to TE=0 to increase signal-to-noise ratio and remove the otherwise remaining R2* bias [10, 24, 57]. The TE=0 extrapolated MTw, PDw and T1w images were used to calculate MT saturation, R1 and apparent signal amplitude A* maps. PD map was derived from A* map, which is proportional to proton density. All quantitative maps were corrected for inhomogeneities from local RF transmit field (B1+), and R1 quantitative maps were further corrected for imperfect RF spoiling using the strategy of Preibisch and Deichmann [58]. The receive bias field map (B1-) was used to correct PD maps for instrumental biases. The R2* map was estimated from all three multi-echo series (MTw, PDw and R1w) using the ESTATICS model [57].

After generating quantitative maps using the hMRI toolbox for all sessions, spatial preprocessing involved the following steps (Figure 1): within-patient registration brought the two serial MR data sets into the individual T0 space, using the longitudinal registration tool from SPM [59]. For each individual patient, a preliminary WM lesion mask was generated based on FLAIR and T1w images by the lesion growth algorithm implemented in the LST

toolbox [56], followed by manual corrections by an MS expert (EL) to remove aberrant/artefactual lesion detections [24]. The images were then segmented using the USwL toolbox, which consists of an extended version of the traditional Unified Segmentation (US) algorithm [60] and includes an additional tissue class representing the WM lesion(s). The US-with-lesion method internally generates a subject-specific extended set of tissue probability maps (TPM) [61]: an extra tissue class, based on the smoothed preliminary lesion mask warped into template space (using cost function masking during normalization [62]), is added to account for the lesion, and the original white matter prior map is updated accordingly [63]. The grey matter TPM was not updated due to a very low number of lesions present in the cortical ribbon. Multi-channel segmentation was conducted, using MTsat, PD, R1 and FLAIR images. This pipeline did not use the PD-, T1- and MT-weighted images acquired for the MPM maps construction, but the parametric maps themselves instead. In this way, voxels do not depict MR intensities but rather physical quantitative parameters. The method generated the segmented tissue classes (*a posteriori* tissue, including lesion, probability maps), as well as spatial warping into standard template space. The preliminary lesion mask was used as input for the first session data (at T0) then the *a posteriori* lesion map generated at this initial step served as prior to the subsequent session (at T1).

Segmentation teased out the different tissue classes of interest: NAWM, NACGM and NADGM, as well as WM lesions. To analyze the microstructure within those tissue classes, *a posteriori* tissue maps were binarized and tissue-specific independent masks were constructed: each voxel is assigned to one single tissue class with the highest probability for that voxel (provided that this probability was above 0.2). The lesion binary mask was further cleaned for lesions <10mm^3 which likely resulted from segmentation errors. Finally, binarized tissue class masks were in turn applied on the MPM maps to extract voxel values inside them.

2.4 Brain volume change

Volumetric changes were investigated using the USwL *a posteriori* tissue probability maps. The following measures of brain volume were computed for each session of each participant: (1) Total intra-cranial volume (TIV) = volume (NAWM + GM + CSF + lesions), (2) brain parenchymal fraction (BPF) = volume (NAWM + GM + lesions)/TIV, (3) Gray matter fraction (GMF) = volume (GM)/TIV, and (4) lesion fraction (LF) = volume (lesion)/TIV. The percentage of change between both scanning sessions was evaluated for each volumetric measurement, then annualized changes were computed by dividing these measures by scan intervals (in years). Results were directly analysed with a t-test (testing if significantly different from 0 at $p < .05$), but also in the same way as the normal appearing tissues MR parameters in relation to the patients' clinical status (see next section).

2.5 Analysis of normal appearing tissues

The median value of quantitative MRI parameters was extracted from the three normal appearing tissues (NAWM, NACGM and NADGM), and an individual annual rate of change (ARoC) was computed for each parameter in each tissue class, based on the initial and final values and accounting for the time interval (in years) between scans. This rate of change in qMRI parameters served as dependent variable in a general linear model testing the effect of clinical status:

$$Y = \beta_0 + \beta_1 X_{status} + \epsilon$$

Y is the ARoC for a qMRI parameter and tissue class, β's are the regression parameters corresponding to the associated regressor (with β_0 the intercept), and ϵ the residuals. X_{status} is a binary categorical variable representing the patient's disease activity status: a status score of 1 was assigned to patients stable or improving from T0 to T1.

This patient status X_{status} was derived from one score of disease activity: NEDA-3 (No Evidence of Disease Activity [64]), a composite of three related measures of disease activity. A score of 0 was assigned in the presence of new clinical relapses (only concerning RRMS patients) and/or MRI activity (new or enlarged lesions visible on FLAIR T2 or Gadolinium-enhanced images) and/or sustained disability progression over six months based on Expanded Disability Status Scale (EDSS). For both RRMS and PMS patients, disability progression was defined as a 1.0-point increase if the EDSS score was $\leq$ 4.0 at baseline and as a 0.5 point increased if the baseline EDSS score was > 4.0. The threshold of 4.0 was proposed in this study because it is considered as a milestone regarding ambulatory performance.

NEDA-3 and was evaluated at mid- and end-scanning interval, and a final status score of 0 was given only to patients for which disease activity or progression was noted in both cases, indicating a clear progression of the disease over the whole interscan interval.

The influence of several clinical measurements such as 25 FWT, 9HPT and SDMT was also considered to refine the evaluation of disease activity. However complete data were lacking for several patients. Moreover, when available, these additional clinical parameters did not modify the final X_{status}. Longitudinal clinical information allowing to derive the disease activity status for each subject appears in Table 2. Additional clinical information concerning annual relapse rate and treatment administration appears in Supplementary material.

Permutation tests were employed for inferences [65]. R-squared value was tested against computed statistics after permutation of the data. For a number *n* of permutations, the X_{status} values were randomly shuffled (constructing a new regressor written X_{status}^{π}), tested against the unchanged response Y, and generating each time a permuted R-squared value (noted R_{π}, R_{obs} being the true R-squared value computed without permutation of the data).

The condition $X_{status} \neq X_{status}^{\pi}$ is verified at each permutation. After *n* permutations (with *n = 5000* in this study), a *p*-value was computed based on the following formula:

$$p = \frac{\#(R_{\pi} > R_{obs})}{n + 1}$$

which estimates the probability of obtaining R_{obs} under the null hypothesis that *Y* is not correlated to X_{status}. The null hypothesis is rejected if $p < .05$ FDR-corrected for multiple comparisons [66], for the 12 tests performed (3 tissue classes with 4 qMRI parameters).

Two-tailed t-tests were applied *post-hoc* on the significant results of permutation tests to compare the ARoC distribution between disease status, i.e., $X_{status} = 0$ against $X_{status} = 1$. Inferences were conducted at a significance level of .05.

The same pipeline was applied to the brain volumetric changes (BPF, GMF and LF) to test their correlation to the disease activity status.

2.6 Analysis of lesions and peripheral tissues

For white matter lesions analysis, we did not use ARoC but exploited directly the qMRI parameters voxel values. Importantly, with USwL segmentation, the prior lesion mask is only used in a probabilistic way and the estimated posterior lesion map, obtained using MTsat, PD, R1 and FLAIR images, typically showed more extended lesion than clinically visible on the FLAIR image alone. Therefore, we separated focal lesions detected on FLAIR images, with LST segmentation and visual inspection, from their peripheral regions detected on qMRI maps. Two different peripheral regions were considered: one for each time point (T0 and T1). Therefore, at T0, three distinct lesion-related regions were isolated:

- The lesions, as clinically defined, pertaining to hyperintensity on the conventional FLAIR MR image acquired at T0. These are referred to as ‘focal FLAIR lesion’.
- The peripheral region detected on qMRI maps at T0, at the borders of (but not including) the focal FLAIR lesion. Those are referred to as ‘initial peripheral lesion’.

- The peripheral region, detected on qMRI maps at follow up, bordering (but not including) the initial peripheral lesion, further referred to as 'later peripheral lesion'. This was computed by masking out the T1 lesion mask with the T0 lesion mask. This region allows us to determine whether its microstructure at T0 forebodes a full-blown plaque, detectable during follow up. Those sometimes appear hyperintense on FLAIR images.

The three areas were compared between each other and with NAWM, in order to characterize them on a microstructural basis (Figure 2). For an accurate lesion-by-lesion analysis, only enlarging lesions, i.e., present in the three masks, were considered for these comparisons.

NAWM region consisted of all white matter voxels which did not belong to any of the three lesion-related regions. The four areas are not overlapping as no voxel could belong to more than one class at the same time.

For all participants, MTsat, PD, R1 and R2* median values were extracted from each lesion area, considering lesions individually (between 2 and 66 measurements per subject). Similarly, the median qMRI values within NAWM were also extracted (one measurement per subject). These values were extracted from T0 and T1 scans separately. Statistical analyses were performed in SAS 9.4 (SAS Institute, Cary, NC). None of the qMRI parameter was normally distributed, therefore we applied a log transformation on each of them prior to statistical analysis. For each qMRI parameter, a separate Generalized Linear Mixed Model (GLMM) tested the effect of areas (NAWM and the three lesion-related areas), and time points (T0 and T1), as well as their interaction (i.e., area*time), on the median qMRI parameter value, with a first-order autoregressive variance/covariance model and participants as a random factor (intercept). The degrees of freedom were estimated using Kenward-Roger's method. Statistical significance was estimated at $p < .05$ after adjustment for multiple comparison using Tukey's procedure.

3. Results

3.1 Volume changes

Brain parenchymal fraction (BPF) annually decreased between T0 and T1 by -0.67 ± 1.12% (significantly different from zero; paired-sample t-tests; $t(16) = 2.57; p = .0204$) whereas lesion fraction (LF) increased by 22.88 ± 26.13% ($t(16) = -3.70; p = .0019$). GM fraction (GMF) non-significantly decreased by -0.30 ± 1.44%.

3.2 Analysis of normal appearing tissues

As expected, changes in MTsat and R2* within normal appearing brain tissues (NABT) between T0 and T1 varied across subjects (Figure 3). PD and R1 exhibited similar behaviors, see Supplementary data.

At the group level, with the regression analysis and permutation inference, we observed that the annual rate of change (ARoC) of MTsat and R2* positively regressed with disease status as follows (Table 3): MTsat in NAWM and NACGM and R2* in NAWM significantly increased in patients who fare well ($X_{status} = 1$).

Post-hoc t-tests applied on these significant results for a clearer illustration of the difference in disease status (Figure 4) were all significant at a level of .05.

Regarding BPF and LF, their correlation to the disease activity status was not significant (Table 3), suggesting that qMRI parameters are more sensitive to subtle microstructural changes in normal appearing tissues over time than global morphological measurements

3.3 Analysis of lesion microstructure

The number of enlarging WM lesions between T0 and T1 varied from 2 to 66 across patients, for a total of 741 identified enlarging lesions among all subject, corresponding on average among patients to 63% (±31%) of the amount of initial focal lesions. The number of enlarging

lesions did not significantly differ between patients' disease status groups ($t(15) = .244, p = .811$).

GLMMs found a significant effect of areas (3 lesion regions and NAWM) for MTsat, R1, R2* and PD median (MTsat: $F_3 = 35.34,\ p < .0001$, PD: $F_3 = 68.03,\ p < .0001$, R1: $F_3 = 40.26,\ p < .0001$, R2*: $F_3 = 32.32,\ p < .0001$). By contrast, neither time effect (T0 vs T1; MTsat: $F_3 = 0.36,\ p = .5481$, PD: $F_3 = 1.20,\ p = .2735$, R1: $F_3 = 2.05,\ p = .1520$, R2*: $F_3 = 2.86,\ p = .0911$), nor the area*time interaction (MTsat: $F_3 = 0.09,\ p = .9671$, PD: $F_3 = 0.14,\ p = .9346$, R1: $F_3 = 0.14,\ p = .9331$, R2*: $F_3 = 0.40,\ p = .7565$) were significant, suggesting the microstructural stability of the initial lesion core. *Post-hoc* tests confirmed significant differences between the four tissue areas.

At times T0 and T1, MTsat, R1 and R2* values were significantly larger in the initial peripheral lesion than FLAIR lesion, in the later peripheral lesion than the initial one, and in the NAWM than later peripheral lesion. The reverse was observed for PD. The significant difference in parameters between initial and later peripheral lesion at T0 suggests that subtle microstructural changes appear in the periphery of the initial lesion, months before their detection as focal FLAIR lesions at T1. Adjusted *p*-values appear in Figure 5. Detailed statistical results of the GLMM's appear in Supplementary data.

4. Discussion

This longitudinal study followed up volumetric data and qMRI brain metrics (MTsat, PD, R1, R2*) in 17 patients with multiple sclerosis for a median time interval of 30 months. The main results are threefold. First, the microstructure of normal appearing brain tissues changes over time and these modifications concur with, and potentially drive, clinical evolution. This critical finding suggests that repair mechanism and edema resorption can be monitored *in vivo*. Second, the microstructure within WM plaques is remarkably heterogeneous. Importantly, at

their periphery, microstructural alterations foreshadow their expansion, as detected by conventional MRI. Third, as expected, we observed a small but significant brain atrophy and lesion load increase with time.

Quantitative MRI parameter time course within NABT

In this study, we used a multiparameter mapping protocol that was gradually optimized and validated for multi-centric studies [67]. It provides high-resolution maps of multiple qMRI parameters from data acquired during a single scanning session of acceptable duration. A number of cross-sectional studies using a combination of MT, R1, R2* or PD parameters reported significant changes in the microstructure of NABT in MS [24-32]. By contrast, longitudinal analyses of multiparameter qMRI data are scarce. A progressive shortening of T2/T2* [68] or increase in R2* [33-35] was reported within the basal ganglia, suggesting increased of myelin and/or iron contents as well as edema resorption. Likewise, PD and T1 increased within a year, suggesting a demyelination and/or axonal loss [36]. MTR progressively decreases in NAWM of MS patients over one [37] or two years [38]. These abnormalities tend to be more pronounced in progressive phenotypes [69] and were associated to a slow, diffuse and global myelin pathology.

Here, we showed that MTsat within NAWM and NACGM and R2* values within NAWM increase in clinically stable or improving patients. Because MTsat and R2* both correlate with myelin content [11, 47, 70-73], our results suggest repair mechanisms within NABT of patients who are responding to disease modifying treatments, despite the initial myelin/axonal loss and independently from WM focal lesion evolution. Such increases could also be explained by an edema/inflammation resorption, but less likely than myelin/axonal density changes since MTsat is the least dependent to water content among the four qMRI parameters. These results echo cross-sectional analyses showing that healthy controls (HC) have higher MTsat

and R2* values within the same tissue classes compared to MS patients [24]. Annual rates of change of R1 and PD within NABT were not significantly associated with the individual clinical status in this study, although R1 reduction within NABT has already been reported in cross sectional [24, 29, 30] and longitudinal [36] studies comparing MS subjects to HC.

Lesion microstructure

Focal inflammatory demyelinating lesions have been extensively characterized and are traditionally classified as active, chronic active (smoldering) or inactive plaques according to the presence and distribution of plaque-infiltrating macrophages/microglia [74-76]]. Focal WM pathology is a constantly evolving process including episodes of demyelination and remyelination but also accumulation of irreversible axonal damage. Age, disease duration, clinical phenotype as well as disease modifying treatment all contribute to the dynamic nature of focal WM pathology [75, 77]. This accounts for the large inter- and intra-individual heterogeneity of MS, which conventional MRI is largely unable to capture. By contrast, quantitative MRI parameters are sensitive to myelin, axonal as well as iron contents and appear as promising markers of plaque dynamics. For instance, MTR was shown to sharply decrease within gadolinium enhancing lesions before recovering during the subsequent months [39-41]. Likewise, reduction of MTR within NAWM, days to weeks before the formation of a new active lesion was also demonstrated [42, 43], and long-term MTR changes in WM plaques were observed in relation with disease progression [69, 78]. The present study broadens the quantitative characterization of plaque dynamics, in keeping with previous longitudinal studies [68, 79]. Two important findings emerge from the results. First, qMRI refines lesion segmentation, as compared to the processing based on the sole FLAIR image. In consequence, the initial lesion revealed by qMRI is typically wider that the plaque detected in FLAIR. Its periphery is characterized by a decrease in MTsat and R2* as compared to NAWM,

suggesting an incipient demyelination, reminiscent of the so-called 'periplaques' [80]. Moreover, MTsat, R2* and R1 values progressively decrease from NAWM to plaque core, suggesting a centripetal loss of myelin content. Second, plaque microstructure is altered in plaque periphery before any observable change in conventional MRI signals. This finding suggests, in keeping with neuropathological observations [75, 77, 81, 82] that subclinical ongoing inflammation and/or demyelination takes place in the periphery of an active plaque, well before it is detectable on FLAIR or T1 post-gadolinium sequences. If confirmed on larger population samples, this finding might significantly modify treatment management in MS patients.

Another plausible hypothesis explaining the progressive decrease of R2* in initial and later peripheral regions is that iron-containing macrophages could be removing iron from the lesions through perivascular drainage into the extracellular compartment. Previous neuropathological studies have reported an iron loss at the edges of a subset of MS lesions, depending on their type (active, inactive, smoldering, etc.) as well as the patient's age and disease duration [83, 84]. Due to the limited sensitivity of R2* to local iron concentration as compared, for example, to the combined use of R2* and quantitative susceptibility mapping (QSM) [18], validating this theory would require additional measures which can better describe iron dynamics in MS lesions and NAWM.

Volumetric Data

CNS atrophy occurs in all stages of MS, since the preclinical phase of the disease and progresses throughout its course, at a much higher rate than one reported in normal aging [85-88]. In this study, the annual brain percentage volume loss at the group level was 0.67%, which is in line with previous publications [89]. We also showed a significant increase in lesion fraction. Volumetric data (ARoC's) were highly variable across subjects: changes in BPF range

from -2.52 to 1.17% and LF from -0.78 to 103.06%. This variability arises from a large number of factors which do not necessarily relate to MS: age, disease duration, disease phenotype, disease modifying treatment, circadian rhythm, hydration… [87, 88]. Moreover, annual changes in brain parenchymal fraction as well as lesion fraction only partially correlated to patients' disease status, in accordance with a large amount of publications [36, 90]. This highlights the lack of specificity and sensitivity of volumetric measurements, at least at the individual level.

It can appear odd that brain atrophy progresses in parallel to repair mechanisms, as suggested by qMRI parameters. However, BPF reduction is minimal, and is not significant (see Table 3) between T0 and T1. One should keep in mind that cortical atrophy is an irreversible phenomenon. Given the inter- and intra-individual heterogeneity of MS progression, it is possible that patients who have undergone neuron- axonal loss at some point in the disease might be able to remyelinize their remaining axons, hopefully through therapeutic intervention or lifestyle changes. Besides, axonal remyelination is not always effective. Here we showed that variations in MTsat and R2* correlated to the disease activity status, but our clinical evaluation based on EDSS is undoubtedly imprecise. Once again, the size and heterogeneity of our cohort limits the interpretation of such results.

Study limitation

As mentioned here above, the small size and heterogeneous aspect of the present dataset constitute major limitations of this study. Indeed, it is composed of only 17 patients, with a rather broad range of characteristics such as age, disease duration, disease phenotype, disease modifying treatment, etc., which are known to influence the disability state of the patient and thus their ability to put together repair mechanisms within cerebral tissues [1, 75-77, 91, 92]. In addition, the time interval between two scanning sessions varied rather widely

across patients (between 14 and 61 months), although it was brought back to an annual rate where possible. All of these parameters were imposed by standard clinical follow up. Therefore, these results should not be over-interpreted but are nevertheless promising and call for a replication with a larger and more homogeneous or controlled set of MS patients. Larger longitudinal studies are currently being held and will probably confirm these preliminary results.

A second limitation is the absence of longitudinal MRI data acquired in a control group of healthy subjects. However, we considered that literature of longitudinal studies of healthy subjects that analysed tissue microstructure could constitute a solution for comparison with MS patients. For example, in Bonnier et al. (2017) [68], the control group did not show any significant differences regarding T1, T2* or MTR measurements over two years, and the median age of their group is quite similar to ours (34,3 vs 36 years). Also, in Elkady et al. (2018) [33], they found no longitudinal R2* effect in their control groups, even with an age range superior to ours. Moreover, the median age of our population (< 60 years), as well as the short period between two scanning sessions (median of 14 months), suggests that microstructural alterations would not be noticeable in a healthy participants group, as many quantitative ageing studies detected differences over much larger time periods [44, 70, 93].

5. Conclusion

These preliminary results highlight the relevance of multiple qMRI data in the monitoring of MS disease, highlighting subtle changes within NABT and plaque dynamics in relation with repair or disease progression. Of course, large scale longitudinal study would be needed to reproduce these findings and better exploit the full potential of qMRI parameters.

References

[1] Lassmann, Hans. “Pathology and Disease Mechanisms in Different Stages of Multiple Sclerosis.” *Journal of the Neurological Sciences* 333, no. 1–2 (October 2013): 1–4. https://doi.org/10.1016/j.jns.2013.05.010.

[2] Trapp, Bruce D., John Peterson, Richard M. Ransohoff, Richard Rudick, Sverre Mörk, and Lars Bö. “Axonal Transection in the Lesions of Multiple Sclerosis.” *New England Journal of Medicine* 338, no. 5 (January 29, 1998): 278–85. https://doi.org/10.1056/NEJM199801293380502.

[3] Haider, Lukas, Tobias Zrzavy, Simon Hametner, Romana Höftberger, Francesca Bagnato, Günther Grabner, Siegfried Trattnig, Sabine Pfeifenbring, Wolfgang Brück, and Hans Lassmann. “The Topograpy of Demyelination and Neurodegeneration in the Multiple Sclerosis Brain.” *Brain* 139, no. 3 (March 2016): 807–15. https://doi.org/10.1093/brain/awv398.

[4] Kutzelnigg, Alexandra, Claudia F. Lucchinetti, Christine Stadelmann, Wolfgang Brück, Helmut Rauschka, Markus Bergmann, Manfred Schmidbauer, Joseph E. Parisi, and Hans Lassmann. “Cortical Demyelination and Diffuse White Matter Injury in Multiple Sclerosis.” *Brain* 128, no. 11 (November 1, 2005): 2705–12. https://doi.org/10.1093/brain/awh641.

[5] Gh Popescu, Bogdan F, and Claudia F Lucchinetti. “Meningeal and Cortical Grey Matter Pathology in Multiple Sclerosis.” *BMC Neurology* 12, no. 1 (December 2012): 11. https://doi.org/10.1186/1471-2377-12-11.

[6] Frischer, Josa M., Stephan Bramow, Assunta Dal-Bianco, Claudia F. Lucchinetti, Helmut Rauschka, Manfred Schmidbauer, Henning Laursen, Per Soelberg Sorensen, and Hans Lassmann. “The Relation between Inflammation and Neurodegeneration in Multiple Sclerosis Brains.” *Brain* 132, no. 5 (May 2009): 1175–89. https://doi.org/10.1093/brain/awp070.

[7] Brown, Robert A., Sridar Narayanan, and Douglas L. Arnold. “Imaging of Repeated Episodes of Demyelination and Remyelination in Multiple Sclerosis.” *NeuroImage: Clinical* 6 (2014): 20–25. https://doi.org/10.1016/j.nicl.2014.06.009.

[8] Wang, Chenyu Tim, Michael Barnett, and Yael Barnett. “Imaging the Multiple Sclerosis Lesion: Insights into Pathogenesis, Progression and Repair.” *Current Opinion in Neurology* 32, no. 3 (June 2019): 338–45. https://doi.org/10.1097/WCO.0000000000000698.

[9] Thompson, Alan J, Brenda L Banwell, Frederik Barkhof, William M Carroll, Timothy Coetzee, Giancarlo Comi, Jorge Correale, et al. “Diagnosis of Multiple Sclerosis: 2017 Revisions of the McDonald Criteria.” *The Lancet Neurology* 17, no. 2 (February 2018): 162–73. https://doi.org/10.1016/S1474-4422(17)30470-2.

[10] Tabelow, Karsten, Evelyne Balteau, John Ashburner, Martina F. Callaghan, Bogdan Draganski, Gunther Helms, Ferath Kherif, et al. “HMRI – A Toolbox for Quantitative MRI in Neuroscience and Clinical Research.” *NeuroImage* 194 (July 2019): 191–210. https://doi.org/10.1016/j.neuroimage.2019.01.029.

[11] Schmierer, Klaus, Francesco Scaravilli, Daniel R. Altmann, Gareth J. Barker, and David H. Miller. “Magnetization Transfer Ratio and Myelin in Postmortem Multiple Sclerosis Brain.” *Annals of Neurology* 56, no. 3 (September 2004): 407–15. https://doi.org/10.1002/ana.20202.

[12] Callaghan, Martina F., Gunther Helms, Antoine Lutti, Siawoosh Mohammadi, and Nikolaus Weiskopf. “A General Linear Relaxometry Model of R $_1$ Using Imaging Data: General Linear Relaxometry Model of R1.” *Magnetic Resonance in Medicine* 73, no. 3 (March 2015): 1309–14. https://doi.org/10.1002/mrm.25210.

[13] Van Waesberghe, J. H. T. M., W. Kamphorst, C. J. A. De Groot, M. A. A. Van Walderveen, J. A. Castelijns, R. Ravid, G. J. Lycklama a Nijeholt, et al. “Axonal Loss in Multiple Sclerosis Lesions: Magnetic Resonance Imaging Insights into Substrates of Disability.” *Annals of Neurology* 46, no. 5 (November 1999): 747–54. https://doi.org/10.1002/1531-8249(199911)46:5<747::AID-ANA10>3.0.CO;2-4.

[14] Mottershead, J. P., K. Schmierer, M. Clemence, J. S. Thornton, F. Scaravilli, G. J. Barker, P. S. Tofts, et al. “High Field MRI Correlates of Myelin Content and Axonal Density in Multiple Sclerosis.” *Journal of Neurology* 250, no. 11 (November 1, 2003): 1293–1301. https://doi.org/10.1007/s00415-003-0192-3.

[15] Lema, Alfonso, Courtney Bishop, Omar Malik, Miriam Mattoscio, Rehiana Ali, Richard Nicholas, Paolo A. Muraro, Paul M. Matthews, Adam D. Waldman, and Rexford D. Newbould. “A Comparison of Magnetization Transfer Methods to Assess Brain and Cervical Cord

Microstructure in Multiple Sclerosis: MT of Brain and c-Spine in MS." *Journal of Neuroimaging* 27, no. 2 (March 2017): 221–26. https://doi.org/10.1111/jon.12377.

[16] Helms, Gunther, Henning Dathe, and Peter Dechent. "Modeling the Influence of TR and Excitation Flip Angle on the Magnetization Transfer Ratio (MTR) in Human Brain Obtained from 3D Spoiled Gradient Echo MRI." *Magnetic Resonance in Medicine* 64, no. 1 (July 2010): 177–85. https://doi.org/10.1002/mrm.22379.

[17] Bagnato, Francesca, Simon Hametner, Emma Boyd, Verena Endmayr, Yaping Shi, Vasiliki Ikonomidou, Guanhua Chen, et al. "Untangling the R2* Contrast in Multiple Sclerosis: A Combined MRI-Histology Study at 7.0 Tesla." Edited by Quan Jiang. *PLOS ONE* 13, no. 3 (March 21, 2018): e0193839. https://doi.org/10.1371/journal.pone.0193839.

[18] Hametner, Simon, Verena Endmayr, Andreas Deistung, Pilar Palmrich, Max Prihoda, Evelin Haimburger, Christian Menard, et al. "The Influence of Brain Iron and Myelin on Magnetic Susceptibility and Effective Transverse Relaxation - A Biochemical and Histological Validation Study." *NeuroImage* 179 (October 2018): 117–33. https://doi.org/10.1016/j.neuroimage.2018.06.007.

[19] Stüber, Carsten, Markus Morawski, Andreas Schäfer, Christian Labadie, Miriam Wähnert, Christoph Leuze, Markus Streicher, et al. "Myelin and Iron Concentration in the Human Brain: A Quantitative Study of MRI Contrast." *NeuroImage* 93 (June 2014): 95–106. https://doi.org/10.1016/j.neuroimage.2014.02.026.

[20] Stankiewicz, James M., Mohit Neema, et Antonia Ceccarelli. « Iron and Multiple Sclerosis ». *Neurobiology of Aging* 35 (September 2014): S51-58. https://doi.org/10.1016/j.neurobiolaging.2014.03.039.

[21] Granziera, Cristina, Jens Wuerfel, Frederik Barkhof, Massimiliano Calabrese, Nicola De Stefano, Christian Enzinger, Nikos Evangelou, et al. "Quantitative Magnetic Resonance Imaging towards Clinical Application in Multiple Sclerosis." *Brain* 144, no. 5 (June 22, 2021): 1296–1311. https://doi.org/10.1093/brain/awab029.

[22] Kolb, Hadar, Martina Absinta, Erin S. Beck, Seung-Kwon Ha, Yeajin Song, Gina Norato, Irene Cortese, Pascal Sati, Govind Nair, and Daniel S. Reich. "7T MRI Differentiates Remyelinated from Demyelinated Multiple Sclerosis Lesions." *Annals of Neurology* 90, no. 4 (October 2021): 612–26. https://doi.org/10.1002/ana.26194.

[23] Edwards, Luke J., Evgeniya Kirilina, Siawoosh Mohammadi, and Nikolaus Weiskopf. "Microstructural Imaging of Human Neocortex in Vivo." *NeuroImage* 182 (November 2018): 184–206. https://doi.org/10.1016/j.neuroimage.2018.02.055.

[24] Lommers, Emilie, Jessica Simon, Gilles Reuter, Gaël Delrue, Dominique Dive, Christian Degueldre, Evelyne Balteau, Christophe Phillips, and Pierre Maquet. "Multiparameter MRI Quantification of Microstructural Tissue Alterations in Multiple Sclerosis." *NeuroImage: Clinical* 23 (2019): 101879. https://doi.org/10.1016/j.nicl.2019.101879.

628 [25] Lommers, Emilie, Camille Guillemin, Gilles Reuter, Eve Fouarge, Gaël Delrue, Fabienne
629 Collette, Christian Degueldre, Evelyne Balteau, Pierre Maquet, and Christophe Phillips. "VOXEL-
630 BASED Quantitative MRI Reveals Spatial Patterns of Grey Matter Alteration in Multiple
631 Sclerosis." *Human Brain Mapping* 42, no. 4 (March 2021): 1003–12.
632 https://doi.org/10.1002/hbm.25274.
633
634 [26] Andica, Christina, Akifumi Hagiwara, Koji Kamagata, Kazumasa Yokoyama, Keigo Shimoji,
635 Asami Saito, Yuki Takenaka, et al. "Gray Matter Alterations in Early and Late Relapsing-
636 Remitting Multiple Sclerosis Evaluated with Synthetic Quantitative Magnetic Resonance
637 Imaging." *Scientific Reports* 9, no. 1 (December 2019): 8147. https://doi.org/10.1038/s41598-
638 019-44615-3.
639
640 [27] Bonnier, Guillaume, Alexis Roche, David Romascano, Samanta Simioni, Djalel Meskaldji,
641 David Rotzinger, Ying-Chia Lin, et al. "Advanced MRI Unravels the Nature of Tissue Alterations
642 in Early Multiple Sclerosis." *Annals of Clinical and Translational Neurology* 1, no. 6 (June 2014):
643 423–32. https://doi.org/10.1002/acn3.68.
644
645 [28] Engström, Maria, Jan B. M. Warntjes, Anders Tisell, Anne-Marie Landtblom, and Peter
646 Lundberg. "Multi-Parametric Representation of Voxel-Based Quantitative Magnetic
647 Resonance Imaging." Edited by Friedemann Paul. *PLoS ONE* 9, no. 11 (November 13, 2014):
648 e111688. https://doi.org/10.1371/journal.pone.0111688.
649
650 [29] Gracien, René-Maxime, Alina Jurcoane, Marlies Wagner, Sarah C. Reitz, Christoph Mayer,
651 Steffen Volz, Stephanie-Michelle Hof, et al. "Multimodal Quantitative MRI Assessment of

652 Cortical Damage in Relapsing-Remitting Multiple Sclerosis: Cortical Quantitative MRI in
653 RRMS." *Journal of Magnetic Resonance Imaging* 44, no. 6 (December 2016): 1600–1607.
654 https://doi.org/10.1002/jmri.25297.
655
656 [30] Neema, Mohit, James Stankiewicz, Ashish Arora, Venkata S.R. Dandamudi, Courtney E.
657 Batt, Zachary D. Guss, Ali Al-Sabbagh, and Rohit Bakshi. "T1- and T2-Based MRI Measures of
658 Diffuse Gray Matter and White Matter Damage in Patients with Multiple Sclerosis." *Journal of*
659 *Neuroimaging* 17 (April 2007): 16S-21S. https://doi.org/10.1111/j.1552-6569.2007.00131.x.
660
661 [31] Reitz, Sarah C., Stephanie-Michelle Hof, Vinzenz Fleischer, Alla Brodski, Adriane Gröger,
662 René-Maxime Gracien, Amgad Droby, et al. "Multi-Parametric Quantitative MRI of Normal
663 Appearing White Matter in Multiple Sclerosis, and the Effect of Disease Activity on T2." *Brain*
664 *Imaging and Behavior* 11, no. 3 (June 2017): 744–53. https://doi.org/10.1007/s11682-016-
665 9550-5.
666
667 [32] Stevenson, V.L, G.J.M Parker, G.J Barker, K Birnie, P.S Tofts, D.H Miller, and A.J Thompson.
668 "Variations in T1 and T2 Relaxation Times of Normal Appearing White Matter and Lesions in
669 Multiple Sclerosis." *Journal of the Neurological Sciences* 178, no. 2 (September 2000): 81–87.
670 https://doi.org/10.1016/S0022-510X(00)00339-7.
671
672 [33] Elkady, Ahmed M., Dana Cobzas, Hongfu Sun, Gregg Blevins, and Alan H. Wilman.
673 "Discriminative Analysis of Regional Evolution of Iron and Myelin/Calcium in Deep Gray Matter
674 of Multiple Sclerosis and Healthy Subjects: Analysis of Iron and Myelin in MS." *Journal of*

675 *Magnetic Resonance Imaging* 48, no. 3 (September 2018): 652–68.
676 https://doi.org/10.1002/jmri.26004.
677
678 [34] Elkady, Ahmed M., Dana Cobzas, Hongfu Sun, Peter Seres, Gregg Blevins, and Alan H.
679 Wilman. "Five Year Iron Changes in Relapsing-Remitting Multiple Sclerosis Deep Gray Matter
680 Compared to Healthy Controls." *Multiple Sclerosis and Related Disorders* 33 (August 2019):
681 107–15. https://doi.org/10.1016/j.msard.2019.05.028.
682
683 [35] Khalil, M., C. Langkammer, A. Pichler, D. Pinter, T. Gattringer, G. Bachmaier, S. Ropele, S.
684 Fuchs, C. Enzinger, and F. Fazekas. "Dynamics of Brain Iron Levels in Multiple Sclerosis: A
685 Longitudinal 3T MRI Study." *Neurology* 84, no. 24 (June 16, 2015): 2396–2402.
686 https://doi.org/10.1212/WNL.0000000000001679.
687
688 [36] Gracien, René-Maxime, Sarah C. Reitz, Stephanie-Michelle Hof, Vinzenz Fleischer, Amgad
689 Droby, Mathias Wahl, Helmuth Steinmetz, Sergiu Groppa, Ralf Deichmann, and Johannes C.
690 Klein. "Longitudinal Quantitative MRI Assessment of Cortical Damage in Multiple Sclerosis: A
691 Pilot Study: Longitudinal Cortical QMRI in MS." *Journal of Magnetic Resonance Imaging* 46,
692 no. 5 (November 2017): 1485–90. https://doi.org/10.1002/jmri.25685.
693
694 [37] Laule, Cornelia, I. M. Vavasour, K. P. Whittall, J. Oger, D. W. Paty, D. K. B. Li, A. L. MacKay,
695 and D. L. Arnold. "Evolution of Focal and Diffuse magnetisation Transfer Abnormalities in
696 Multiple Sclerosis." *Journal of Neurology* 250, no. 8 (August 2003): 924–31.
697 https://doi.org/10.1007/s00415-003-1115-z.
698

[38] Hayton, T., J. Furby, K. J. Smith, D. R. Altmann, R. Brenner, J. Chataway, K. Hunter, D. J. Tozer, D. H. Miller, and R. Kapoor. “Longitudinal Changes in Magnetisation Transfer Ratio in Secondary Progressive Multiple Sclerosis: Data from a Randomised Placebo Controlled Trial of Lamotrigine.” *Journal of Neurology* 259, no. 3 (March 2012): 505–14. https://doi.org/10.1007/s00415-011-6212-9.

[39] Dousset, Vincent, Annick Gayou, Bruno Brochet, and Jean-Marie Caille. “Early Structural Changes in Acute MS Lesions Assessed by Serial Magnetization Transfer Studies.” *Neurology* 51, no. 4 (October 1998): 1150–55. https://doi.org/10.1212/WNL.51.4.1150.

[40] Levesque, Ives R., Paul S. Giacomini, Sridar Narayanan, Luciana T. Ribeiro, John G. Sled, Doug L. Arnold, and G. Bruce Pike. “Quantitative Magnetization Transfer and Myelin Water Imaging of the Evolution of Acute Multiple Sclerosis Lesions: Quantitative MT and T_2 in Acute MS Lesions.” *Magnetic Resonance in Medicine* 63, no. 3 (March 2010): 633–40. https://doi.org/10.1002/mrm.22244.

[41] Elskamp, Ij van den, Dl Knol, H. Vrenken, G. Karas, A. Meijerman, M. Filippi, L. Kappos, et al. “Lesional Magnetization Transfer Ratio: A Feasible Outcome for Remyelinating Treatment Trials in Multiple Sclerosis.” *Multiple Sclerosis Journal* 16, no. 6 (June 2010): 660–69. https://doi.org/10.1177/1352458510364630.

[42] Filippi, Massimo, Maria A. Rocca, Gianvito Martino, Mark A. Horsfield, and Giancarlo Comi. “Magnetization Transfer Changes in the Normal Appering White Matter Precede the

722 Appearance of Enhancing Lesions in Patients with Multiple Sclerosis." *Annals of Neurology* 43,
723 no. 6 (June 1998): 809–14. https://doi.org/10.1002/ana.410430616.
724
725 [43] Fazekas, F, S Ropele, C Enzinger, T Seifert, and S Strasser-Fuchs. "Quantitative
726 Magnetization Transfer Imaging of Pre-Lesional White-Matter Changes in Multiple Sclerosis."
727 *Multiple Sclerosis Journal* 8, no. 6 (December 2002): 479–84.
728 https://doi.org/10.1191/1352458502ms860oa.
729
730 [44] Draganski, B., J. Ashburner, C. Hutton, F. Kherif, R.S.J. Frackowiak, G. Helms, and N.
731 Weiskopf. "Regional Specificity of MRI Contrast Parameter Changes in Normal Ageing
732 Revealed by Voxel-Based Quantification (VBQ)." *NeuroImage* 55, no. 4 (April 2011): 1423–34.
733 https://doi.org/10.1016/j.neuroimage.2011.01.052.
734
735 [45] Polman, Chris H., Stephen C. Reingold, Brenda Banwell, Michel Clanet, Jeffrey A. Cohen,
736 Massimo Filippi, Kazuo Fujihara, et al. "Diagnostic Criteria for Multiple Sclerosis: 2010
737 Revisions to the McDonald Criteria." *Annals of Neurology* 69, no. 2 (February 2011): 292–302.
738 https://doi.org/10.1002/ana.22366.
739
740 [46] Guillemin, C., E. Lommers, G. Delrue, E. Gester, P. Maquet, et F. Collette. « The Complex
741 Interplay Between Trait Fatigue and Cognition in Multiple Sclerosis ». *Psychologica Belgica* 62,
742 nº 1 (March 2022): 108. https://doi.org/10.5334/pb.1125.
743
744

[47] Carey, Daniel, Francesco Caprini, Micah Allen, Antoine Lutti, Nikolaus Weiskopf, Geraint Rees, Martina F. Callaghan, and Frederic Dick. “Quantitative MRI Provides Markers of Intra-, Inter-Regional, and Age-Related Differences in Young Adult Cortical Microstructure.” *NeuroImage* 182 (November 2018): 429–40. https://doi.org/10.1016/j.neuroimage.2017.11.066.

[48] Reuter, Gilles, Emilie Lommers, Evelyne Balteau, Jessica Simon, Christophe Phillips, Felix Scholtes, Didier Martin, Arnaud Lombard, and Pierre Maquet. “Multiparameter Quantitative Histological MRI Values in High-Grade Gliomas: A Potential Biomarker of Tumor Progression.” *Neuro-Oncology Practice* 7, no. 6 (December 4, 2020): 646–55. https://doi.org/10.1093/nop/npaa047.

[49] Depierreux, Frédérique, Eric Parmentier, Laurane Mackels, Katherine Baquero, Christian Degueldre, Evelyne Balteau, Eric Salmon, et al. “Parkinson’s Disease Multimodal Imaging: F-DOPA PET, Neuromelanin-Sensitive and Quantitative Iron-Sensitive MRI.” *Npj Parkinson’s Disease* 7, no. 1 (December 2021): 57. https://doi.org/10.1038/s41531-021-00199-2.

[50] Nürnberger, Lucas, René-Maxime Gracien, Pavel Hok, Stephanie-Michelle Hof, Udo Rüb, Helmuth Steinmetz, Rüdiger Hilker, Johannes C. Klein, Ralf Deichmann, and Simon Baudrexel. “Longitudinal Changes of Cortical Microstructure in Parkinson’s Disease Assessed with T1 Relaxometry.” *NeuroImage: Clinical* 13 (2017): 405–14. https://doi.org/10.1016/j.nicl.2016.12.025.

[51] Klein, J.C., M. Rolinski, L. Griffanti, K. Szewczyk-Krolikowski, F. Baig, C. Ruffmann, A.R. Groves, R.A.L. Menke, M.T. Hu, and C. Mackay. “Cortical Structural Involvement and Cognitive Dysfunction in Early Parkinson’s Disease.” *NMR in Biomedicine* 31, no. 4 (April 2018): e3900. https://doi.org/10.1002/nbm.3900.

[52] Lutti, Antoine, Chloe Hutton, Jürgen Finsterbusch, Gunther Helms, and Nikolaus Weiskopf. “Optimization and Validation of Methods for Mapping of the Radiofrequency Transmit Field at 3T: Optimized RF Transmit Field Mapping at 3T.” *Magnetic Resonance in Medicine* 64, no. 1 (July 2010): 229–38. https://doi.org/10.1002/mrm.22421.

[53] Lutti, Antoine, Joerg Stadler, Oliver Josephs, Christian Windischberger, Oliver Speck, Johannes Bernarding, Chloe Hutton, and Nikolaus Weiskopf. “Robust and Fast Whole Brain Mapping of the RF Transmit Field B1 at 7T.” Edited by Wang Zhan. *PLoS ONE* 7, no. 3 (March 12, 2012): e32379. https://doi.org/10.1371/journal.pone.0032379.

[54] Filippi, M., Rocca, M. A., Horsfield, M. A., Hametner, S., Geurts, J. J., Comi, G., & Lassmann, H. “Imaging cortical damage and dysfunction in multiple sclerosis.” *JAMA neurology*, *70*(5) (May 2013): 556–564. https://doi.org/10.1001/jamaneurol.2013.1954

[55] Hulst, Hanneke E, and Jeroen JG Geurts. “Gray Matter Imaging in Multiple Sclerosis: What Have We Learned?” *BMC Neurology* 11, no. 1 (December 2011): 153. https://doi.org/10.1186/1471-2377-11-153.

792 [56] Schmidt, Paul, Christian Gaser, Milan Arsic, Dorothea Buck, Annette Förschler, Achim
793 Berthele, Muna Hoshi, et al. “An Automated Tool for Detection of FLAIR-Hyperintense White-
794 Matter Lesions in Multiple Sclerosis.” *NeuroImage* 59, no. 4 (February 2012): 3774–83.
795 https://doi.org/10.1016/j.neuroimage.2011.11.032.
796
797 [57] Weiskopf, Nikolaus, Martina F. Callaghan, Oliver Josephs, Antoine Lutti, and Siawoosh
798 Mohammadi. “Estimating the Apparent Transverse Relaxation Time (R2*) from Images with
799 Different Contrasts (ESTATICS) Reduces Motion Artifacts.” *Frontiers in Neuroscience* 8
800 (September 10, 2014). https://doi.org/10.3389/fnins.2014.00278.
801
802 [58] Preibisch, C., and R. Deichmann. “Influence of RF Spoiling on the Stability and Accuracy of
803 T_1 Mapping Based on Spoiled FLASH with Varying Flip Angles: Influence of RF Spoiling on T_1
804 Mapping.” *Magnetic Resonance in Medicine* 61, no. 1 (January 2009): 125–35.
805 https://doi.org/10.1002/mrm.21776.
806
807 [59] Ashburner, John. “Symmetric Diffeomorphic Modeling of Longitudinal Structural MRI.”
808 *Frontiers in Neuroscience* 6 (2013). https://doi.org/10.3389/fnins.2012.00197.
809
810 [60] Ashburner, John, and Karl J. Friston. “Unified Segmentation.” *NeuroImage* 26, no. 3 (July
811 2005): 839–51. https://doi.org/10.1016/j.neuroimage.2005.02.018.
812
813 [61] Lorio, S., S. Fresard, S. Adaszewski, F. Kherif, R. Chowdhury, R.S. Frackowiak, J. Ashburner,
814 et al. “New Tissue Priors for Improved Automated Classification of Subcortical Brain Structures

on MRI." *NeuroImage* 130 (April 2016): 157–66. https://doi.org/10.1016/j.neuroimage.2016.01.062.

[62] Andersen, Sarah M., Steven Z. Rapcsak, and Pélagie M. Beeson. "Cost Function Masking during Normalization of Brains with Focal Lesions: Still a Necessity?" *NeuroImage* 53, no. 1 (October 2010): 78–84. https://doi.org/10.1016/j.neuroimage.2010.06.003.

[63] Moon, Nathan, Elizabeth Bullitt, Koen van Leemput, and Guido Gerig. "Automatic Brain and Tumor Segmentation." In *Medical Image Computing and Computer-Assisted Intervention — MICCAI 2002*, edited by Takeyoshi Dohi and Ron Kikinis, 2488:372–79. Lecture Notes in Computer Science. Berlin, Heidelberg: Springer Berlin Heidelberg, 2002. https://doi.org/10.1007/3-540-45786-0_46.

[64] Pandit, Lekha. "No Evidence of Disease Activity (NEDA) in Multiple Sclerosis - Shifting the Goal Posts." *Annals of Indian Academy of Neurology* 22, no. 3 (2019): 261. https://doi.org/10.4103/aian.AIAN_159_19.

[65] Anderson, Marti J. "Permutation Tests for Univariate or Multivariate Analysis of Variance and Regression." *Canadian Journal of Fisheries and Aquatic Sciences* 58, no. 3 (March 1, 2001): 626–39. https://doi.org/10.1139/f01-004.

[66] Yoav Benjamini and Yosef Hochberg. "Controlling the False Discovery Rate: a Practical and Powerful Approach to Multiple Testing" *Journal of the Royal Statistical Society. Series B (Methodological)*, Vol. 57, No.1 (1995), 289-300.

[67] Leutritz, Tobias, Maryam Seif, Gunther Helms, Rebecca S Samson, Armin Curt, Patrick Freund, and Nikolaus Weiskopf. “Multiparameter Mapping of Relaxation (R1 , R2 *), Proton Density and Magnetization Transfer Saturation at 3 T : A Multicenter Dual-vendor Reproducibility and Repeatability Study.” *Human Brain Mapping* 41, no. 15 (October 15, 2020): 4232–47. https://doi.org/10.1002/hbm.25122.

[68] Bonnier, Guillaume, Benedicte Maréchal, Mário João Fartaria, Pavel Falkowskiy, José P. Marques, Samanta Simioni, Myriam Schluep, et al. “The Combined Quantification and Interpretation of Multiple Quantitative Magnetic Resonance Imaging Metrics Enlightens Longitudinal Changes Compatible with Brain Repair in Relapsing-Remitting Multiple Sclerosis Patients.” *Frontiers in Neurology* 8 (September 27, 2017): 506. https://doi.org/10.3389/fneur.2017.00506.

[69] Rocca, Maria A, Giovanna Mastronardo, Mariemma Rodegher, Giancarlo Comi, and Massimo Filippi. “Long-Term Changes of Magnetization Transfer-Derived Measures from Patients with Relapsing-Remitting and Secondary Progressive Multiple Sclerosis,” *AJNR Am J Neuroradiol* 20 (1999):821–827

[70] Callaghan, Martina F., Patrick Freund, Bogdan Draganski, Elaine Anderson, Marinella Cappelletti, Rumana Chowdhury, Joern Diedrichsen, et al. “Widespread Age-Related Differences in the Human Brain Microstructure Revealed by Quantitative Magnetic Resonance Imaging.” *Neurobiology of Aging* 35, no. 8 (August 2014): 1862–72. https://doi.org/10.1016/j.neurobiolaging.2014.02.008.

[71] Weiskopf, Nikolaus, Siawoosh Mohammadi, Antoine Lutti, and Martina F. Callaghan. "Advances in MRI-Based Computational Neuroanatomy: From Morphometry to in-Vivo Histology." *Current Opinion in Neurology* 28, no. 4 (August 2015): 313–22. https://doi.org/10.1097/WCO.0000000000000222.

[72] Hametner, Simon, Verena Endmayr, Andreas Deistung, Pilar Palmrich, Max Prihoda, Evelin Haimburger, Christian Menard, et al. "The Influence of Brain Iron and Myelin on Magnetic Susceptibility and Effective Transverse Relaxation - A Biochemical and Histological Validation Study." *NeuroImage* 179 (October 2018): 117–33. https://doi.org/10.1016/j.neuroimage.2018.06.007.

[73] Mangeat, G., S.T. Govindarajan, C. Mainero, and J. Cohen-Adad. "Multivariate Combination of Magnetization Transfer, T 2 * and B0 Orientation to Study the Myelo-Architecture of the in Vivo Human Cortex." *NeuroImage* 119 (October 2015): 89–102. https://doi.org/10.1016/j.neuroimage.2015.06.033.

[74] Dutta, R., and B. D. Trapp. "Pathogenesis of Axonal and Neuronal Damage in Multiple Sclerosis." *Neurology* 68, no. Issue 22, Supplement 3 (May 29, 2007): S22–31. https://doi.org/10.1212/01.wnl.0000275229.13012.32.

[75] Frischer, Josa M., Stephen D. Weigand, Yong Guo, Nilufer Kale, Joseph E. Parisi, Istvan Pirko, Jay Mandrekar, et al. "Clinical and Pathological Insights into the Dynamic Nature of the

White Matter Multiple Sclerosis Plaque: Dynamic Nature of MS Plaque." *Annals of Neurology* 78, no. 5 (November 2015): 710–21. https://doi.org/10.1002/ana.24497.

[76] Lassmann, Hans, Wolfgang Brück, and Claudia Lucchinetti. "Heterogeneity of Multiple Sclerosis Pathogenesis: Implications for Diagnosis and Therapy." *Trends in Molecular Medicine* 7, no. 3 (March 2001): 115–21. https://doi.org/10.1016/S1471-4914(00)01909-2.

[77] Lucchinetti, Claudia, Wolfgang Brück, Joseph Parisi, Bernd Scheithauer, Moses Rodriguez, and Hans Lassmann. "Heterogeneity of Multiple Sclerosis Lesions: Implications for the Pathogenesis of Demyelination." *Annals of Neurology* 47, no. 6 (June 2000): 707–17. https://doi.org/10.1002/1531-8249(200006)47:6<707::AID-ANA3>3.0.CO;2-Q.

[78] Zheng, Yufan, Jar-Chi Lee, Richard Rudick, and Elizabeth Fisher. "Long-Term Magnetization Transfer Ratio Evolution in Multiple Sclerosis White Matter Lesions: Long-Term MTR Evolution in MS WM Lesions." *Journal of Neuroimaging* 28, no. 2 (March 2018): 191–98. https://doi.org/10.1111/jon.12480.

[79] Chawla, Sanjeev, Ilya Kister, Tim Sinnecker, Jens Wuerfel, Jean-Christophe Brisset, Friedemann Paul, and Yulin Ge. "Longitudinal Study of Multiple Sclerosis Lesions Using Ultra-High Field (7T) Multiparametric MR Imaging." Edited by Quan Jiang. *PLOS ONE* 13, no. 9 (September 13, 2018): e0202918. https://doi.org/10.1371/journal.pone.0202918.

[80] Lieury, Alice, Marie Chanal, Géraldine Androdias, Richard Reynolds, Sylvie Cavagna, Pascale Giraudon, Christian Confavreux, and Serge Nataf. "Tissue Remodeling in Periplaque

910 Regions of Multiple Sclerosis Spinal Cord Lesions: Glia Remodeling in MS Spinal Cord." *Glia* 62,
911 no. 10 (October 2014): 1645–58. https://doi.org/10.1002/glia.22705.
912
913 [81] Kuhlmann, Tanja, Samuel Ludwin, Alexandre Prat, Jack Antel, Wolfgang Brück, and Hans
914 Lassmann. "An Updated Histological Classification System for Multiple Sclerosis Lesions." *Acta*
915 *Neuropathologica* 133, no. 1 (January 2017): 13–24. https://doi.org/10.1007/s00401-016-
916 1653-y.
917
918 [82] Lassmann, Hans, Wolfgang Brück, and Claudia F. Lucchinetti. "The Immunopathology of
919 Multiple Sclerosis: An Overview." *Brain Pathology* 17, no. 2 (April 2007): 210–18.
920 https://doi.org/10.1111/j.1750-3639.2007.00064.x.
921
922 [83] Hametner, Simon, Isabella Wimmer, Lukas Haider, Sabine Pfeifenbring, Wolfgang Brück,
923 and Hans Lassmann. "Iron and Neurodegeneration in the Multiple Sclerosis Brain." *Annals of*
924 *Neurology* 74, no. 6 (December 2013): 848–61. https://doi.org/10.1002/ana.23974.
925
926 [84] Popescu, Bogdan F., Josa M. Frischer, Samuel M. Webb, Mylyne Tham, Reginald C. Adiele,
927 Christopher A. Robinson, Patrick D. Fitz-Gibbon, et al. "Pathogenic Implications of Distinct
928 Patterns of Iron and Zinc in Chronic MS Lesions." *Acta Neuropathologica* 134, no. 1 (July 2017):
929 45–64. https://doi.org/10.1007/s00401-017-1696-8.
930
931 [85] De Stefano, N., A. Giorgio, M. Battaglini, M. Rovaris, M. P. Sormani, F. Barkhof, T.
932 Korteweg, et al. "Assessing Brain Atrophy Rates in a Large Population of Untreated Multiple

933 Sclerosis Subtypes." *Neurology* 74, no. 23 (June 8, 2010): 1868–76.
934 https://doi.org/10.1212/WNL.0b013e3181e24136.
935
936 [86] Eshaghi, Arman, Ferran Prados, Wallace J. Brownlee, Daniel R. Altmann, Carmen Tur, M.
937 Jorge Cardoso, Floriana De Angelis, et al. "Deep Gray Matter Volume Loss Drives Disability
938 Worsening in Multiple Sclerosis: Deep Gray Matter Volume Loss." *Annals of Neurology* 83, no.
939 2 (February 2018): 210–22. https://doi.org/10.1002/ana.25145.
940
941 [87] Bermel, Robert A, and Rohit Bakshi. "The Measurement and Clinical Relevance of Brain
942 Atrophy in Multiple Sclerosis." *The Lancet Neurology* 5, no. 2 (February 2006): 158–70.
943 https://doi.org/10.1016/S1474-4422(06)70349-0.
944
945 [88] Zivadinov, R., A. T. Reder, M. Filippi, A. Minagar, O. Stuve, H. Lassmann, M. K. Racke, M.
946 G. Dwyer, E. M. Frohman, and O. Khan. "Mechanisms of Action of Disease-Modifying Agents
947 and Brain Volume Changes in Multiple Sclerosis." *Neurology* 71, no. 2 (July 8, 2008): 136–44.
948 https://doi.org/10.1212/01.wnl.0000316810.01120.05.
949
950 [89] De Stefano, Nicola, Maria Laura Stromillo, Antonio Giorgio, Maria Letizia Bartolozzi,
951 Marco Battaglini, Mariella Baldini, Emilio Portaccio, Maria Pia Amato, and Maria Pia Sormani.
952 "Establishing Pathological Cut-Offs of Brain Atrophy Rates in Multiple Sclerosis." *Journal of*
953 *Neurology, Neurosurgery & Psychiatry*, April 22, 2015, jnnp-2014-309903.
954 https://doi.org/10.1136/jnnp-2014-309903.
955

[90] Christian Enzinger, Frederik Barkhof, Olga Ciccarelli, Massimo Filippi, Ludwig Kappos, Maria A. Rocca, et al. “Nonconventional MRI and Microstructural Cerebral Changes in Multiple Sclerosis.” *Nature Reviews Neurology* 11, no. 12 (December 2015): 676–86. https://doi.org/10.1038/nrneurol.2015.194.

[91] Bodini, Benedetta, Mattia Veronese, Daniel García-Lorenzo, Marco Battaglini, Emilie Poirion, Audrey Chardain, Léorah Freeman, et al. “Dynamic Imaging of Individual Remyelination Profiles in Multiple Sclerosis.” *Annals of Neurology* 79, no. 5 (May 2016): 726–38. https://doi.org/10.1002/ana.24620.

[92] Patrikios, P., C. Stadelmann, A. Kutzelnigg, H. Rauschka, M. Schmidbauer, H. Laursen, P. S. Sorensen, W. Bruck, C. Lucchinetti, and H. Lassmann. “Remyelination Is Extensive in a Subset of Multiple Sclerosis Patients.” *Brain* 129, no. 12 (June 9, 2006): 3165–72. https://doi.org/10.1093/brain/awl217.

[93] Gracien, RM., Nürnberger, L., Hok, P. *et al.* Evaluation of brain ageing: a quantitative longitudinal MRI study over 7 years. *Eur Radiol* **27,** 1568–1576 (2017). https://doi.org/10.1007/s00330-016-4485-1

Tables

	All Patients (n = 17)	
Age, y, median (range)	36 (25-65)	
Sex, F/M	7/10	
MS phenotype (RRMS/MS)	11/6	
Baseline disease duration, y, median (range)	3.4 (0.3-28)	
Baseline EDSS, median (range)	2.5 (1-6.5)	
Baseline number of relapses, median (range)	**RRMS**: 2 (1-5)	**PMS**: N/A
Disease-modifying treatment	**RRMS**: First line, n: 5 Second line, n: 6	**PMS**: Ocrelizumab, n: 2 None, n: 4

Table 1: Demographic data of the study sample

	EDSS T0	EDSS T1/2	New lesion T1/2	Relapse T1/2	NEDA T1/2	EDSS T1	New lesion T1	Relapse T1	NEDA T1	Time period T0-T1	Score
sub-001	2	2	None	None	YES	2	None	None	YES	30	1
sub-002	1.5	1.5	None	None	YES	1.5	None	None	YES	27	1
sub-003	2	2	None	None	YES	2	None	None	YES	27	1
sub-004	3	3	None	None	YES	3.5	None	None	YES	25	1
sub-005	1	1	None	None	YES	1	None	None	YES	24	1
sub-006	1.5	1.5	None	None	YES	1.5	None	None	YES	24	1
sub-007	2	2	None	None	YES	2	None	None	YES	22	1
sub-008	3.5	4.5	None	N/A	NO	5	None	N/A	NO	51	0
sub-009	2	2.5	None	None	YES	2.5	None	None	YES	57	1
sub-010	6	6	Yes	N/A	NO	6.5	None	None	NO	14	0
sub-011	6	6	None	N/A	YES	6.5	None	N/A	NO	14	1
sub-012	1	1.5	None	None	YES	1.5	None	None	YES	55	1
sub-013	5.5	6	None	N/A	NO	6.5	None	N/A	NO	60	0
sub-014	2.5	3.5	Yes	Yes	NO	3	None	None	YES	57	1
sub-015	4	4.5	None	N/A	NO	5	None	N/A	NO	51	0
sub-016	5	4.5	Yes	N/A	NO	4.5	None	N/A	YES	61	1
sub-017	2	3	Yes	Yes	NO	3	Yes	Yes	NO	56	0

Table 2: Longitudinal clinical information and derived disease status score. The time period between T0 and T1 is expressed in months.

	NAWM	NACGM	NADGM
MTsat	**0.039 (.011)***	**0.017 (.007)***	0.004 (.749)
PD	-0.018 (.670)	0.405 (.225)	0.250 (.552)
R1	0.009 (.139)	0.004 (.471)	0.010 (.111)
R2*	**0.295 (.002)***	0.121 (.092)	0.066 (.770)
BPF	-0.884 (.1562)		
LF	21.23 (.1082)		

Table 3: Regression coefficients and their associated *p*-values (in parentheses) for the effects of X_{status} on the individual ARoC for each qMRI parameter (MTsat, PD, R1 and R2*) and for volumetric measurements (BPF and LF).

* Results significant at $p < .05$, FDR corrected.

Legends of figures

Figure 1: Chartflow of data creation and processing (see text). MPM maps were created with the hMRI-toolbox, FLAIR images were directly acquired for both sessions (T0 and T1). A preliminary mask was constructed based on T0 FLAIR. All images (MPM and FLAIR, T0 and T1) were co-registered to the MPM T0 space. Segmentation using USwL allowed to isolate the different tissue classes.

Figure 2: Schematic illustration of the NAWM and 3 lesions-related areas: focal FLAIR lesion (dark gray area), initial peripheral lesion detected at T0 (medium gray area), later peripheral lesion detected at T1 (dashed, left, and light gray, right, area)**.**

Figure 3: Line plots illustrating individual ARoC's for MTsat (left) and R2* (right) in NAWM. Each line corresponds to one subject. Dotted lines represent increasing rates.

Figure 4: Violin plots of significant change rates in microstructure with respect to X_{status}. From left to right: MTsat in NAWM, MTsat in NACGM, R2* in NAWM. * $P < .05$.

Figure 5: Microstructural parameters in NAWM and the 3 lesion-related areas, for each scanning time T0 and T1. P-values were obtained with *post-hoc* tests on the tissue area effect. * $P < .05$.

Appendix A: Supplementary data legends

Supplementary data 1: Multi-echo 3D FLASH acquisition parameters for Siemens Magnetom PRISMA MRI

Supplementary data 2: Extended demographic data. Age, disease duration, EDSS and relapses values were taken at baseline.

Supplementary data 3: Additional follow-up clinical data for each subject.

Supplementary data 4: Line plots illustrating individual ARoC's for PD (left) and R1 (right) in NAWM. Each line corresponds to one subject. Dotted lines represent increasing rates.

Supplementary data 5: Differences of lesion class Least Squares Means. First two columns correspond to tissue class labels (0 = NAWM, 1 = Later peripheral lesion, 2 = Initial peripheral lesion, 3 = FLAIR lesion).

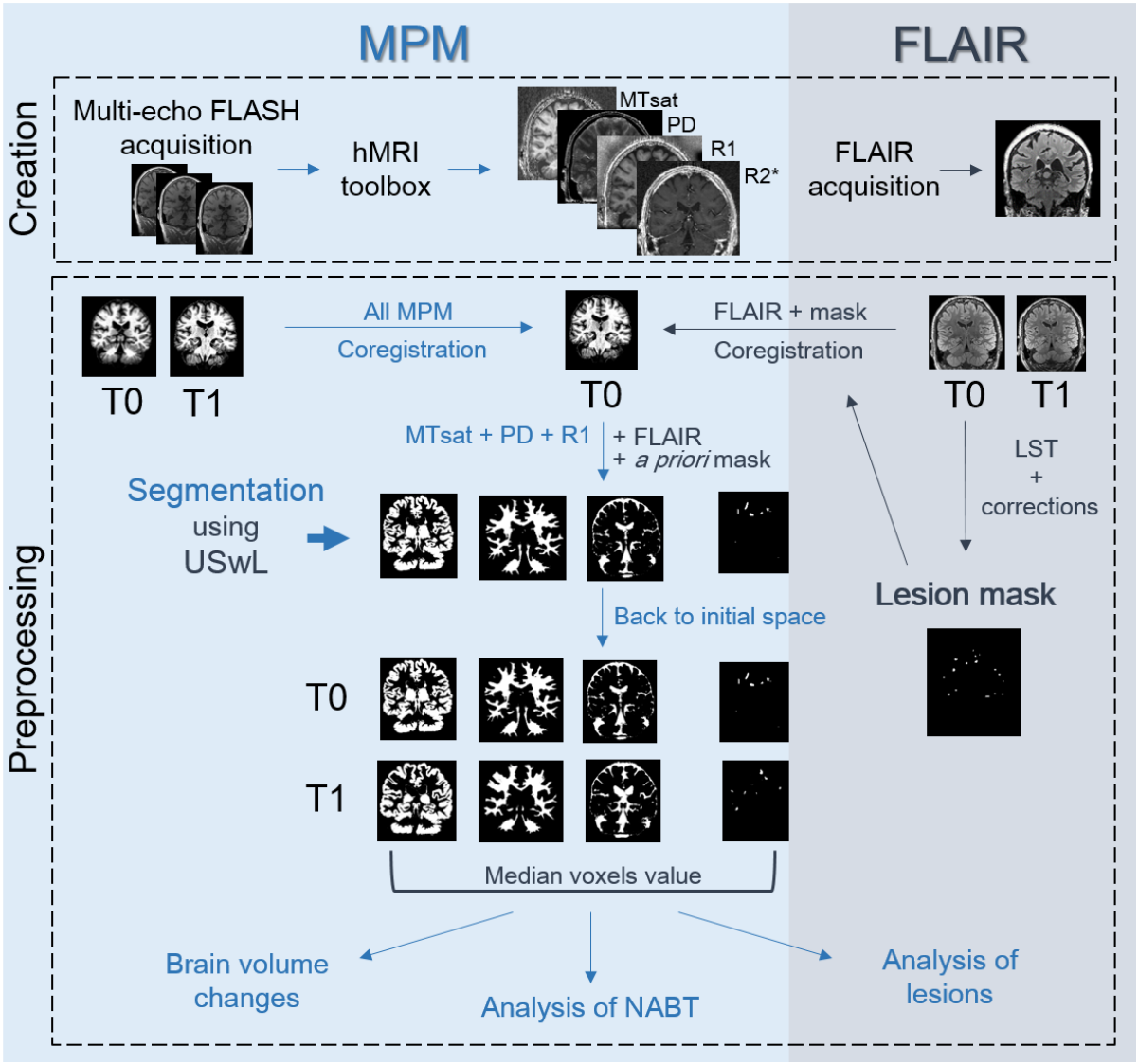

Figure 1: Chartflow of data creation and processing (see text). MPM maps were created with the hMRI-toolbox, FLAIR images were directly acquired for both sessions (T0 and T1). A preliminary mask was constructed based on T0 FLAIR. All images (MPM and FLAIR, T0 and T1) were co-registered to the MPM T0 space. Segmentation using USwL allowed to isolate the different tissue classes.

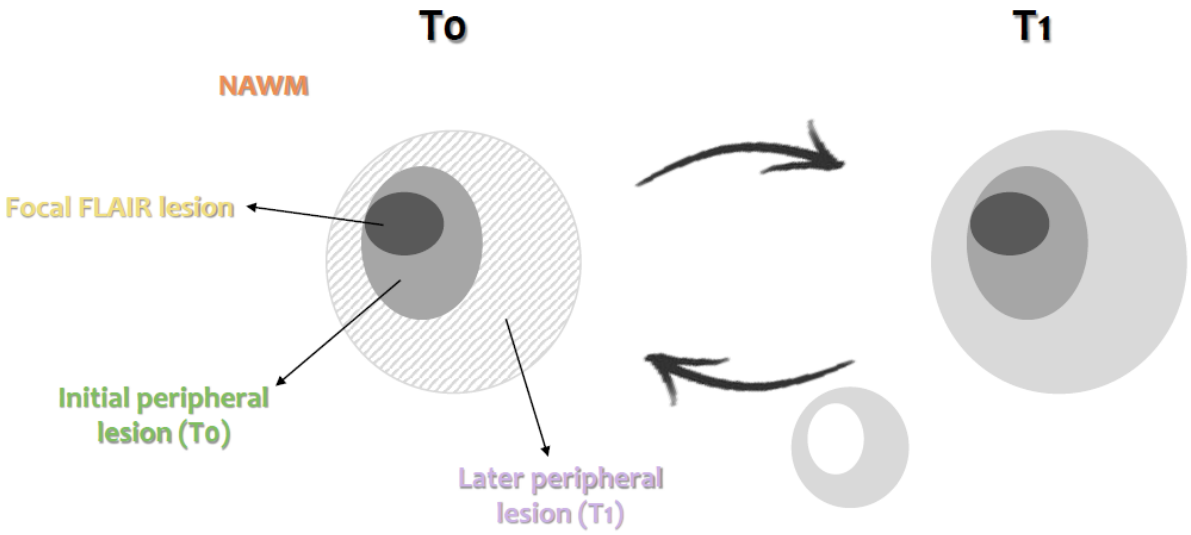

Figure 2: Schematic illustration of the NAWM and 3 lesions-related areas: focal FLAIR lesion (dark gray area), initial peripheral lesion detected at T0 (medium gray area), later peripheral lesion detected at T1 (dashed, left, and light gray, right, area)

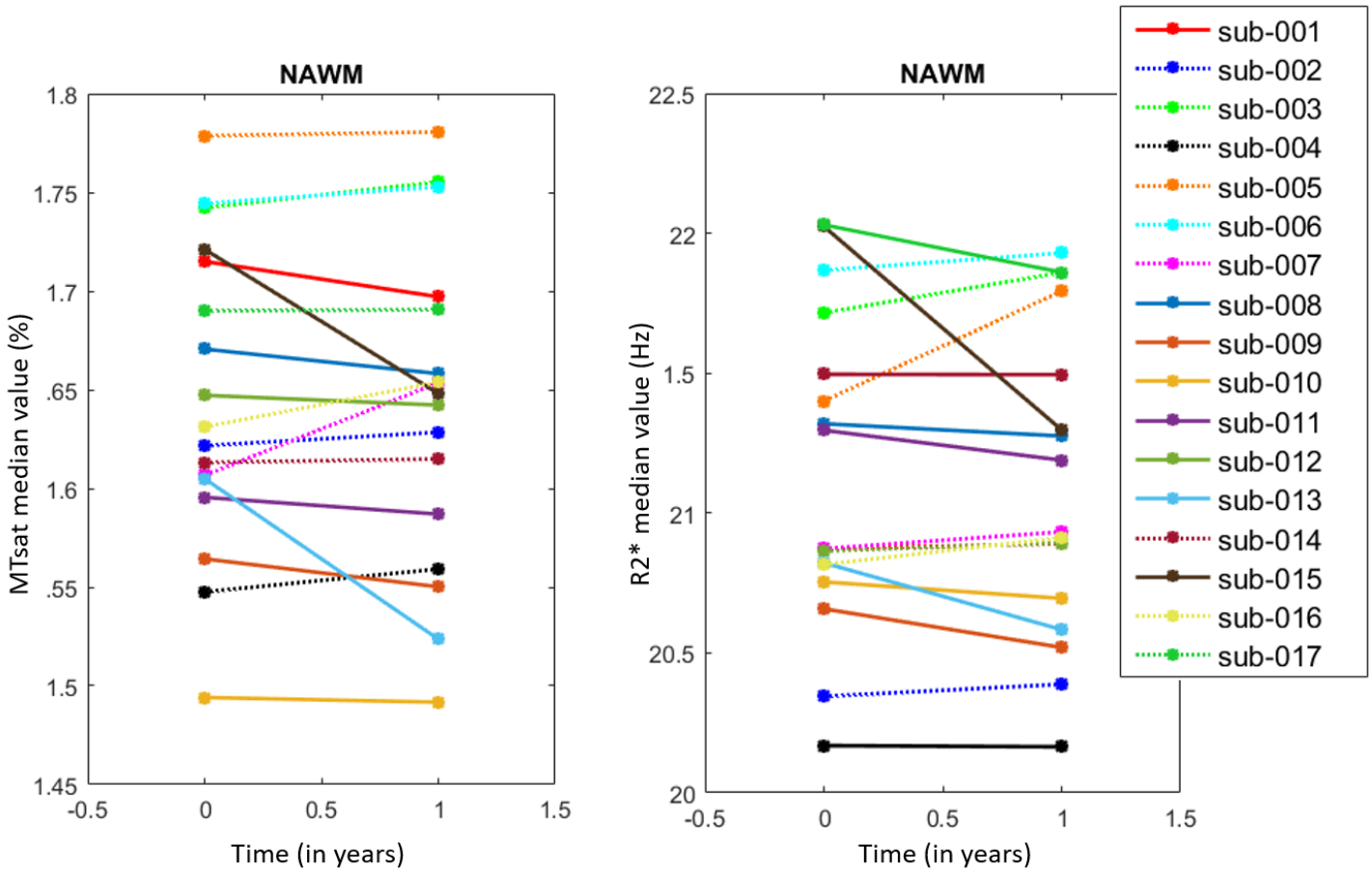

Figure 3: Line plots illustrating individual ARoC's for MTsat (left) and R2* (right) in NAWM.

Each line corresponds to one subject. Dotted lines represent increasing rates.

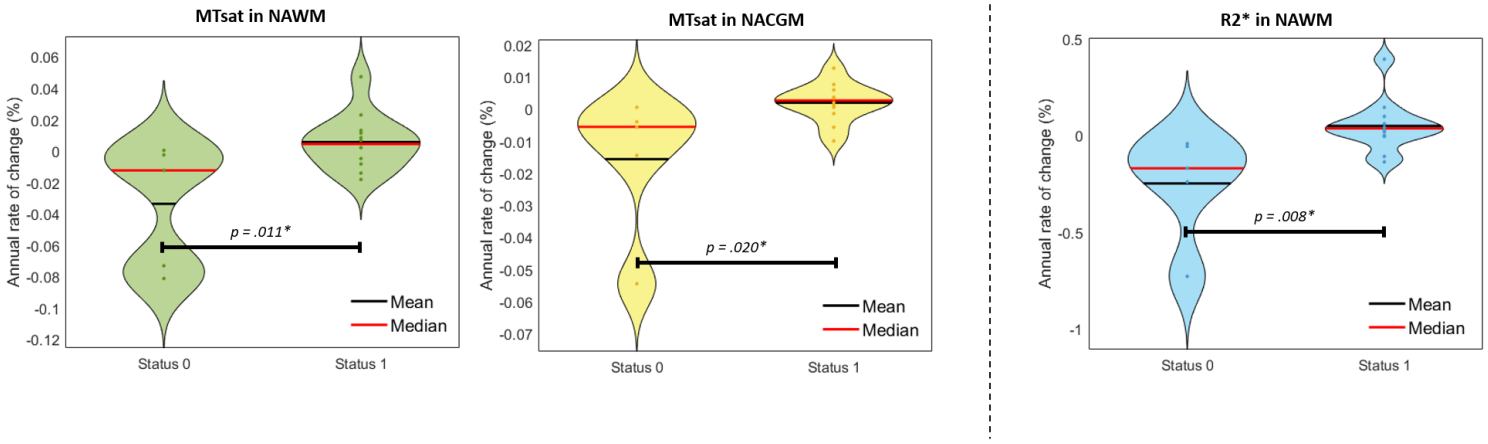

Figure 4: Violin plots of significant change rates in microstructure with respect to X_{status}.

From left to right: MTsat in NAWM, MTsat in NACGM, R2* in NAWM. * $P < .05$.

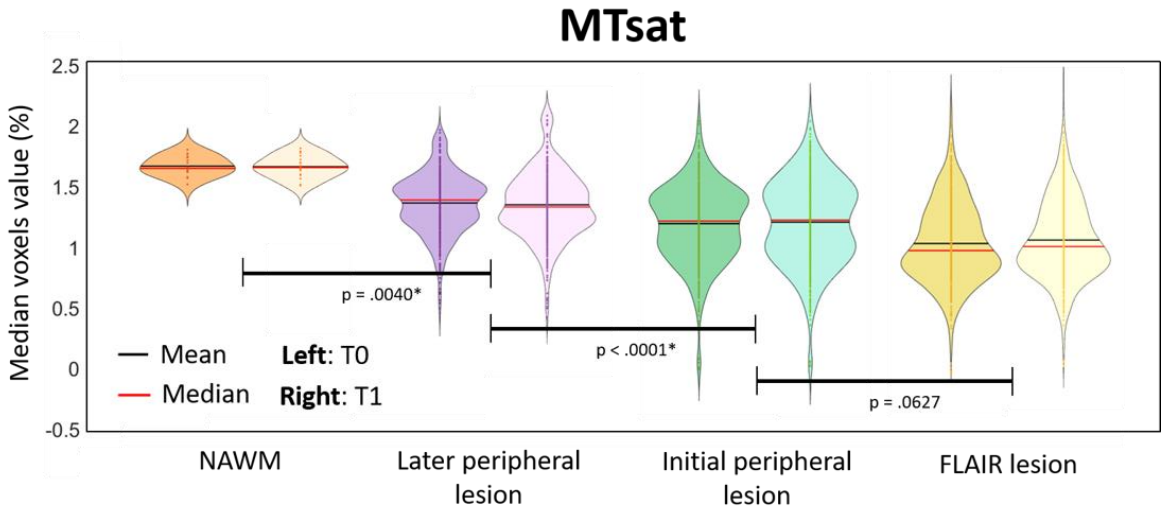
MTsat
Median voxels value (%)
2.5
2
1.5
1
0.5
0
-0.5
p = .0040*
p < .0001*
p = .0627
Mean
Median
Left: T0
Right: T1
NAWM
Later peripheral lesion
Initial peripheral lesion
FLAIR lesion

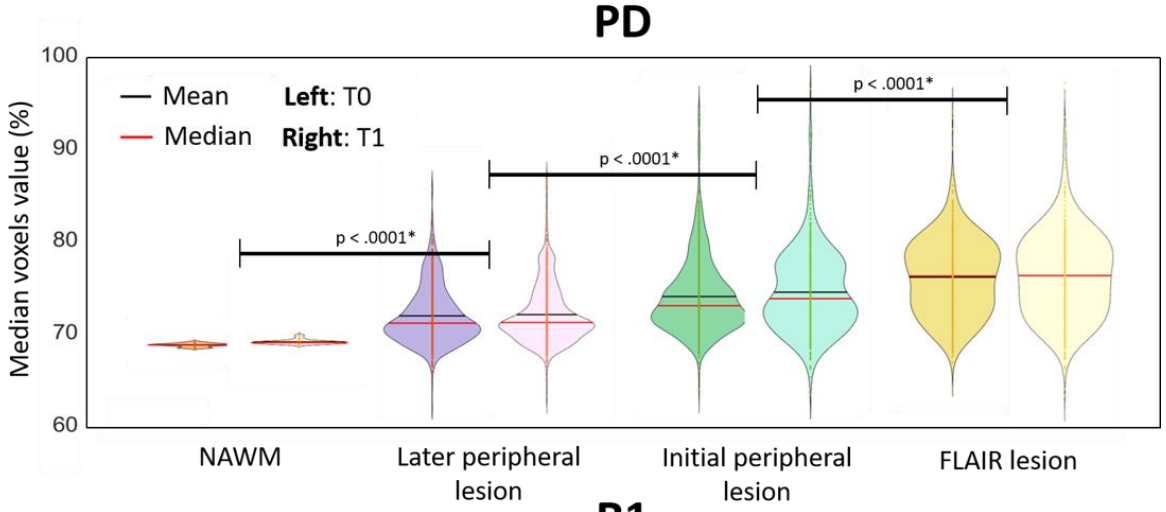
PD
Median voxels value (%)
100
90
80
70
60
p < .0001*
p < .0001*
p < .0001*
Mean
Median
Left: T0
Right: T1
NAWM
Later peripheral lesion
Initial peripheral lesion
FLAIR lesion

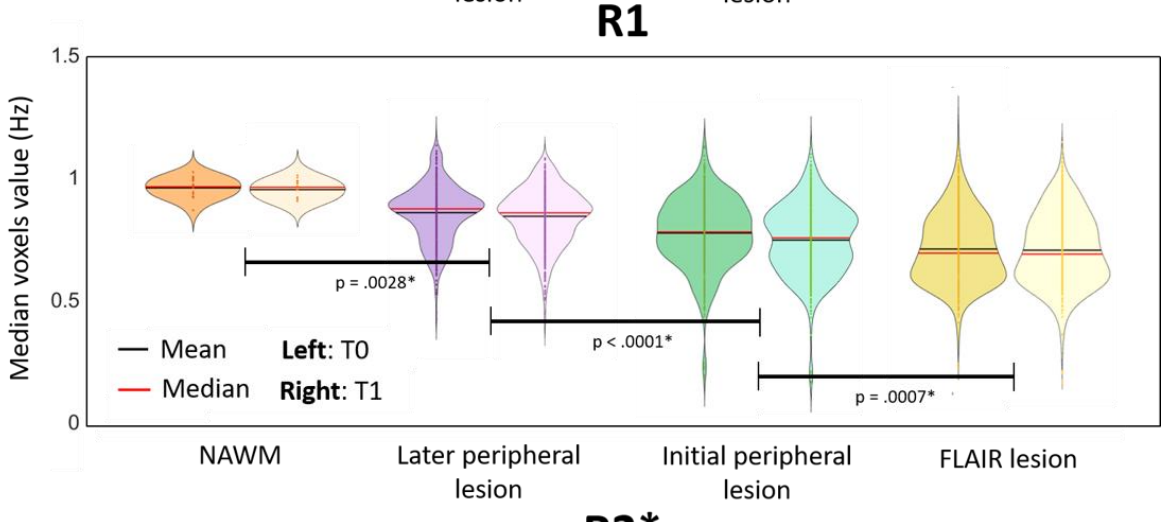
R1
Median voxels value (Hz)
1.5
1
0.5
0
p = .0028*
p < .0001*
p = .0007*
Mean
Median
Left: T0
Right: T1
NAWM
Later peripheral lesion
Initial peripheral lesion
FLAIR lesion

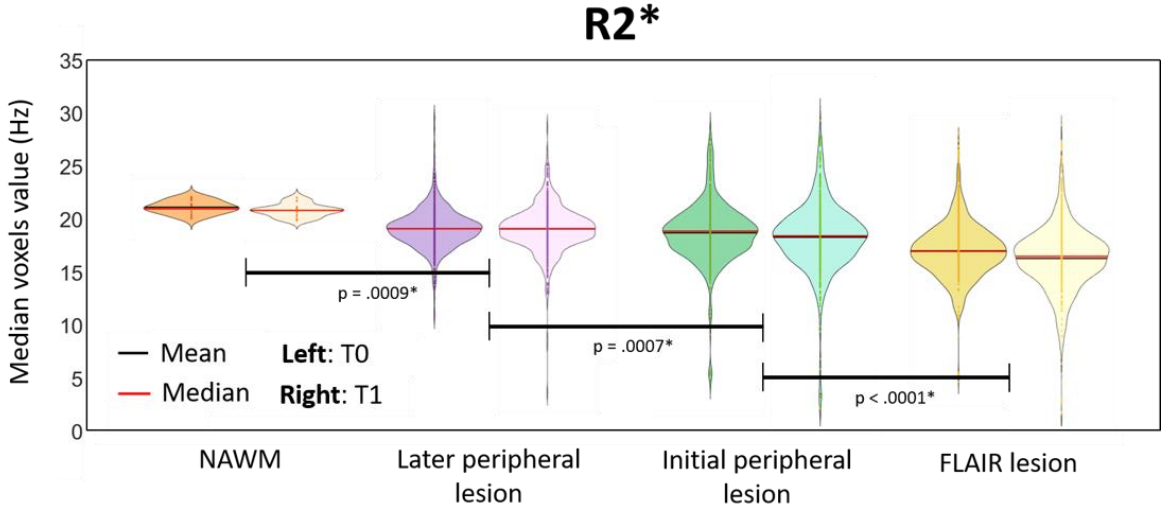
R2*
Median voxels value (Hz)
35
30
25
20
15
10
5
0
p = .0009*
p = .0007*
p < .0001*
Mean
Median
Left: T0
Right: T1
NAWM
Later peripheral lesion
Initial peripheral lesion
FLAIR lesion

Figure 5: Microstructural parameters in NAWM and the 3 lesion-related areas, for each scanning time T0 and T1. P-values were obtained with *post-hoc* tests on the tissue area effect. * $P < .05$.